Water Reuse

Water Reuse Vol 14 No 1, 39 doi: 10.2166/wrd.2024.118

Removal of tellurium(IV) from environmental aquatic systems using metal-organic framework material MIL-100(Fe)

Yiru Huang*, Youyou Li, Qingwei Zhong and Chen Luo

College of Air Traffic Management, Civil Aviation Flight University of China, Sichuan 618307, China
*Corresponding author. E-mail: huangyiru@cafuc.edu.cn

ABSTRACT

Metal-organic framework (MOF) materials, characterized by their porosity and large specific surface areas, exhibit excellent adsorption properties. With the aim of removing Te(IV) from environmental aquatic systems, this study is the first to propose the use of MIL-100(Fe). The material reveals a strong adsorption capacity for Te(IV), with maximum adsorption of 531.9 mg/g, superior to other adsorbent materials. Adsorption isotherm and kinetic models indicate that the adsorption process primarily involves monolayer chemical adsorption. According to the thermodynamic parameters, the adsorption reaction is endothermic. The experiment individually examined factors affecting the material's adsorption performance, including adsorbent dose, initial concentration of Te(IV), pH, adsorption time, and coexisting ions. Even under high ion strength conditions and high concentrations of coexisting ions, the material's adsorption efficiency for Te(IV) still reached over 94%. The material has been successfully applied to remove Te(IV) from lake water, river water, and seawater, yielding satisfactory results. Due to the high salinity and ionic strength of the solution, the removal efficiency of Te(IV) in the seawater matrix was slightly lower than that in freshwater (river and lake water). Thus, this material shows promise for the removal of Te(IV) from complex aquatic systems.

Key words: environmental aquatic, metal-organic framework material, removal, Tellurium(IV)

HIGHLIGHTS

- MIL-100(Fe) was prepared and characterized.
- The Te(IV) can be adsorbed by MIL-100(Fe) effectively, and the adsorption process was primarily a monolayer chemical adsorption and an endothermic reaction.
- The Te(IV) can be removed effectively in environmental water supplies by MIL-100(Fe).

GRAPHICAL ABSTRACT

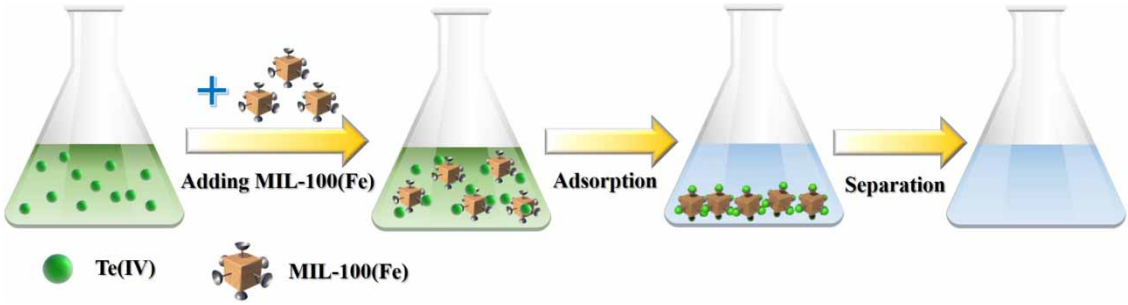

INTRODUCTION

The natural abundance of semi-metal tellurium (Te) in the earth's crust is extremely scarce, only 1–5 μg/kg (Belzile & Chen 2015). Te, as a strategic resource, plays a crucial role in promoting global development and contributing to national economies due to its high commercial and industrial value. It has been applied in numerous industries, comprising photovoltaic

materials, colored glass, electronics, and ceramics (Chen *et al.* 2021; Liu *et al.* 2021). However, with the widespread mining of tellurium ores and the extensive usage of tellurium materials, a significant amount of toxic tellurium-contaminated wastewater has been generated, potentially causing severe pollution and disturbing the ecological balance. In environmental water bodies, tellurium primarily occurs as Te(IV) and Te(VI). Te(IV) exhibits 10 times the toxicity of Te(VI), and it demonstrates a certain degree of toxicity and teratogenicity (Li *et al.* 2021b). Therefore, from the perspective of sustainable development and environmental protection, the removal of highly toxic tellurous acid salts from tellurium-containing wastewater is an urgent issue that needs to be addressed.

Present techniques for removing Te from solutions comprise membrane separation (Li *et al.* 2021c), chemical precipitation (Xu *et al.* 2020), and adsorption (Narimani-Sabegh & Noroozian 2018; Yu *et al.* 2018). Among these, adsorption technology is a common method for removing pollutants from water, playing a crucial role in pollution removal due to its efficiency, simplicity, and reusability. However, the quality of pollutant adsorption performance depends on the characteristics of the adsorbent materials themselves. Common materials for Te removal include TiO_2 (Zhang *et al.* 2010; Qiu *et al.* 2020), ZrO_2 (Wu *et al.* 2018), and magnetic nanoscale zero-valent iron (NZVFe) (Yu *et al.* 2018). Nevertheless, the continuous pursuit of researchers is the discovery of new, efficient, and inexpensive adsorbent materials. A novel kind of organic-inorganic hybrid material that emerged in recent years is metal-organic framework (MOF), which is characterized by huge specific surface areas, large porosity, and tunable morphology (Li *et al.* 2018). MOFs, with the characteristics of both organic polymers and inorganic compounds, have attracted great interest among researchers. They are widely used in magnetic materials, gas storage, sensors, catalysis, and adsorption (Kreno *et al.* 2012; Dubey *et al.* 2017). The structure and properties of MOFs can be adjusted to form new selective adsorbent materials through the selection of distinct metal ions and organic bridging ligands (Hasan & Jhung 2015). In comparison to conventional solid adsorbents (including activated carbon and mesoporous silica materials) (Wang & Dai 2009), MOFs offer further advantages, comprising diverse structural compositions, exposed active sites, adjustable sizes of pores, and huge surface areas. These characteristics provide several occasions for guest molecules to enter the framework and interact with it (Gupta *et al.* 2011), which is conducive to capturing target pollutants to meet the requirement for satisfactory removal efficiency. Specifically, its exceptional performance in removing organic and inorganic pollutants from water bodies has been demonstrated. Extensive research has been conducted on the use of ZIF-8 for arsenic removal (Li *et al.* 2014), FJI-H9 (MOF) for cadmium removal (Xue *et al.* 2016), UiO-66 for mercury removal (Zhao *et al.* 2021), and Zn-MOFs for lead removal (Tahmasebi *et al.* 2015) and organic dyes elimination (Kim *et al.* 2020). Additionally, Fe-based MOF material, MIL-100(Fe), has been successfully applied for arsenic removal due to its unique mesoporous structure, high surface area, and abundant active sites (Cai *et al.* 2016). It has resulted in an impressive adsorption capacity of up to 110 mg/g and excellent performance (Cai *et al.* 2016). However, there is a scarcity of reports concerning the research field of Te removal with MOFs. As iron-based inorganic oxides have some affinity for Te due to their widespread abundance and Te naturally exists in pyrite (Borner *et al.* 2021), the search for the iron-based adsorbent with a unique structure and high capacity to remove highly toxic Te(IV) from environmental water bodies is highly meaningful.

In this experiment, for the first time, we used the MOF material MIL-100(Fe) to remove Te(IV) from the solution. We investigated the performance of this adsorbent material and mainly studied the impacts of the amount of adsorbent, solution's initial pH, initial Te(IV) concentration, and competitive ions on the adsorption performance of MIL-100(Fe). Moreover, to examine the removal of Te(IV) in environmental water bodies by this material, it was applied to remove high concentrations of Te(IV) in lake water, river water, and seawater sample matrices. The removal efficiency of Te(IV) by MIL-100(Fe) was determined. The kinetics and thermodynamics of Te(IV) adsorption were also discussed, providing a deeper understanding of its adsorption mechanism.

EXPERIMENT

Reagents and materials

The experiments utilized only reagents of analytical grade or higher. Deionized water (DIW) was used throughout the experiment for solution preparation. $Fe(NO_3)_3{\cdot}9H_2O$, H_3BTC, and $Na_2TeO_3{\cdot}2H_2O$ were supplied by Aladdin Industrial Corporation (Shanghai, China). $Na_2TeO_3{\cdot}2H_2O$ was used to prepare a 1,000 mg/L Te(IV) standard solution. NaOH, $NaHCO_3$, HCl, HNO_3, HF, KCl, $NaNO_3$, $MgCl_2$, Na_3PO_4, CH_3OH, and $CaCl_2$ were obtained from Cologne Chemicals Limited (Chengdu, Sichuan). 2 mol/L of HCl and 2 mol/L of NaOH were used for pH adjustment of the solution. Lake and river

water samples were collected near Jianyang, Chengdu, and seawater samples were collected from Dalian and Hainan, respectively. Before collecting samples, it is essential to rinse the collection bottle several times with the respective environmental water sample. During sample collection, ensure that the sampling bottle is filled with the water sample to eliminate any air trapped inside. Following collection for later use, all water samples underwent filtration through a 0.45-μm filter membrane for subsequent use. In this experiment, a seawater matrix was employed, which was derived from actual seawater diluted by half. All containers used in this work were soaked overnight with 20% (v/v) HNO_3, followed by rinsed with DIW and dried at 60 °C.

Instruments and characterization

Inductively coupled plasma atomic emission spectrometry (ICP-OES, Avio-500, Perkin-Elmer, USA) was employed for determining the Te(IV). As depicted in Table S1, Supplementary material, the operating parameters were set according to the manufacturer's recommendations. Employing X-ray diffraction (XRD, D8 Advance, Bruker, Germany), the crystal structure of MIL-100(Fe) was characterized and confirmed. N_2 adsorption and desorption analyses were conducted using a Micromeritics ASAP 2020 Plus. Specific surface areas and pore size distributions for the sorbent were estimated utilizing the Brunauer–Emmett–Teller (BET) and the Barrett–Joyner–Halenda (BJH) techniques, respectively. Scanning electron microscopy (SEM, ZEISS sigma500, Germany) and energy dispersive X-ray spectroscopy (EDS, Bruker XFlash 6130, Germany) were employed to determine the morphology and elemental composition of MIL-100(Fe). For the analysis of the alterations in the chemical valence of Te(IV) after adsorption by MIL-100(Fe), X-ray photoelectron spectroscopy (XPS, Thermo Fisher Scientific Escalab 250 Xi, USA) was employed. Fourier transform infrared spectroscopy (FTIR, Thermo Fisher IS20, USA) was utilized to investigate the changes in the chemical bonds of Te(IV) after adsorption by MIL-100(Fe).

Synthesis and characterization of MIL-100(Fe)

Employing a hydrothermal synthesis technique, the synthesis of MIL-100(Fe) was done (Ke *et al.* 2015). The synthesis process was as follows: first, 3.2526 g of $FeCl_3{\cdot}6H_2O$ (12.03 mmol), 0.426 mL of HF, 0.326 mL of HNO_3, and 1.6932 g of H_3BTC (8.06 mmol) had a dissolution in 60 mL of DIW. Then, the solution was stirred for 10 min to ensure homogeneity and transferred to a PTFE-lined stainless steel autoclave, and for 12 h, heating was done at 150 °C. Following the reaction's cooling to room temperature, the product was rinsed three times each with DIW and methanol, and the yellow solid was recovered by filtration. To obtain the resulting MIL-100(Fe) polymer, the overnight drying was done at 150 °C. The XRD was employed to characterize the produced MIL-100(Fe), and its characteristic diffraction peaks were in line with those stated in the literature (as depicted in Figure S1, Supplementary material) (Ke *et al.* 2015). We conducted an analysis on the specific surface area and porosity of the material. As shown in Figures S2 and S3, Supplementary material, the N_2 adsorption-desorption isotherm revealed that the synthetized MIL-100(Fe) has a specific surface area of about 1,554 m^2/g, and a major pore size of approximately 1.5 nm. It indicated that the MIL-100(Fe) possesses favorable mesoporous surface properties, which could provide plenty of active sites for targeted adsorption and promoted the transportation between the adsorbent and the target substance, proving beneficial for the adsorption of Te(IV).

Analytical procedure

To study the adsorption performance of the MOF material MIL-100(Fe) for Te(IV), batch experiments were conducted under different conditions. In the investigation of factors that may influence the removal efficiency of Te(IV) by MIL-100(Fe), a controlled variable method was used for the experiments. Unless specifically stated, all adsorption runs were performed in 250 mL conical flasks at 298 K. In general, 0.5 g/L of MIL-100(Fe) adsorbent was introduced into 50 mL of 50 mg/L Te(IV) solution, and the mixture was sonicated to ensure homogeneity. Subsequently, the mixture was agitated at 25 °C for 2 h on a thermostatic shaker (200 rpm). After shaking, the solid/liquid phases were separated by filtration through a 0.45 μm filter to obtain the supernatant, and 2 mL of this supernatant was taken and added to 2 mL of 4% (v/v) HNO_3 so that the test sample solution contained 2% (v/v) HNO_3. Finally, the solution was analyzed by ICP-OES, and after adsorption, the residual Te(IV) concentration in the sample solution was investigated using a standard curve. All experiments in this work were repeated three times and the obtained experimental results represent the average of the three trials.

Following are the formulae for calculating the adsorbent's removal efficiency (R%) and adsorption capacity (q_e, mg/g):

$$R(\%) = \frac{C_0 - C_e}{C_0} \times 100\% \quad (1)$$

$$q_e = \frac{(C_0 - C_e) \times V}{m} \quad (2)$$

where C_0 and C_e are the initial and equilibrium concentrations of Te(IV) in the solution (mg/L), V (mL) is the volume of sample solution, and m (mg/L) is the amount of adsorbent.

Adsorption kinetics and isotherm models

The adsorption kinetics of Te(IV) on MIL-100(Fe) were determined by monitoring the adsorption efficiency at varying times. The experiments were conducted at an initial Te(IV) concentration of 50 mg/L and a MIL-100(Fe) concentration of 0.5 g/L over various adsorption durations (0–480 min). The equilibrium state of the adsorption process was described by adsorption isotherms. In this experiment, 25.0 mg of MIL-100(Fe) was added to 50 mL solutions of Te(IV) with concentrations ranging from 5 to 2,000 mg/L without adjusted pH. The mixture was shaken for 2 h at a constant temperature of 25 °C. After shaking, the sample solution was filtered through a 0.45 μm filter membrane, and the Te(IV) concentration in the supernatant was measured using ICP-OES. To examine the adsorption isotherms of MIL-100(Fe) for Te(IV), two of the most common isotherm models, the Langmuir and Freundlich models, were applied.

Effect of solution temperature

To investigate the effect of temperature on the removal efficiency of Te(IV) by MIL-100(Fe), it was studied at different temperatures of 25, 35, and 45 °C in the presence of 50 mL of 50 mg/L Te(IV) solution, 25.0 mg of MIL-100(Fe), a reaction time of 2 h, and without adjusted pH.

Impact of other factors on Te removal

In the adsorption experiments, the controlled variable method was used to study the impact of various factors, such as solution pH, adsorption time, adsorbent concentration, and coexisting ions, on the removal efficiency of MIL-100(Fe) for Te(IV). By varying the factor under investigation while holding all other experimental conditions constant, the influence of each factor was explored.

RESULTS AND DISCUSSION

Removal of Te(IV) by MIL-100(Fe)

During solid-phase adsorption, the solution's pH is one of the significant parameters affecting the material's removal efficiency (Yu *et al.* 2020). Therefore, we investigated the adsorption of Te(IV) by MIL-100(Fe) in the pH ranging between 2 and 12 under conditions of an initial 50 mg/L of Te(IV) concentration, 0.5 g/L of adsorbent dosage, and a solution volume of 50 mL. As shown in Figure 1(a), in the pH range of 2–6, the removal efficiency of MIL-100(Fe) for Te(IV) gradually increases with the increase in pH. The zeta potential of MIL-100(Fe) was positively charged at pH < 4 and negatively charged at pH > 4 (Jun *et al.* 2015). Therefore, the reason for the low removal efficiency at lower pH values (pH = 2–6) may be due to the 'acid effect', where Te(IV) mainly exists in water solution in the form of uncharged H_2TeO_3 and negatively charged $HTeO_3^-$, thereby weakening the electrostatic attraction between the adsorbent and the target substance Te(IV) (Li *et al.* 2021b). Thus, electrostatic interactions may be involved in the adsorption process (Wang *et al.* 2022). Subsequently, as the pH increases (pH = 6–12), Te(IV) mainly exists in the form of oxygen-containing anions ($HTeO_3^-$ and/or TeO_3^{2-}), while the zeta potential of MIL-100(Fe) exhibits a negative trend. Thereby it could increase the electrostatic repulsion between the adsorbent and Te(IV). However, in the pH range of 6–12, MIL-100(Fe) has a removal efficiency of over 96% for Te(IV) (Figure 1(a)). This may imply that MIL-100(Fe) removing the pollutant Te(IV) efficiently was not solely dependent on electrostatic interactions. To further understand this process, an additional experiment was conducted subsequently. FTIR spectra of MIL-100(Fe) before and after Te(IV) adsorption was recorded (as shown in Figure S4, Supplementary material). A new small absorption peak was observed at approximately 620 cm^{-1} after the adsorption of Te(IV), which may be owed to the stretching vibration band of the Te(IV)–O bond (Arab *et al.* 2017; Wu *et al.* 2018). Therefore, chemisorption was also one of the ways in which MIL-100(Fe) adsorbs Te(IV). The results showed a broad pH range for the removal of Te(IV) by this material, which included the pH range of general environmental waters. For the sake of simplicity in experimental operation, subsequent experiments did not adjust the pH.

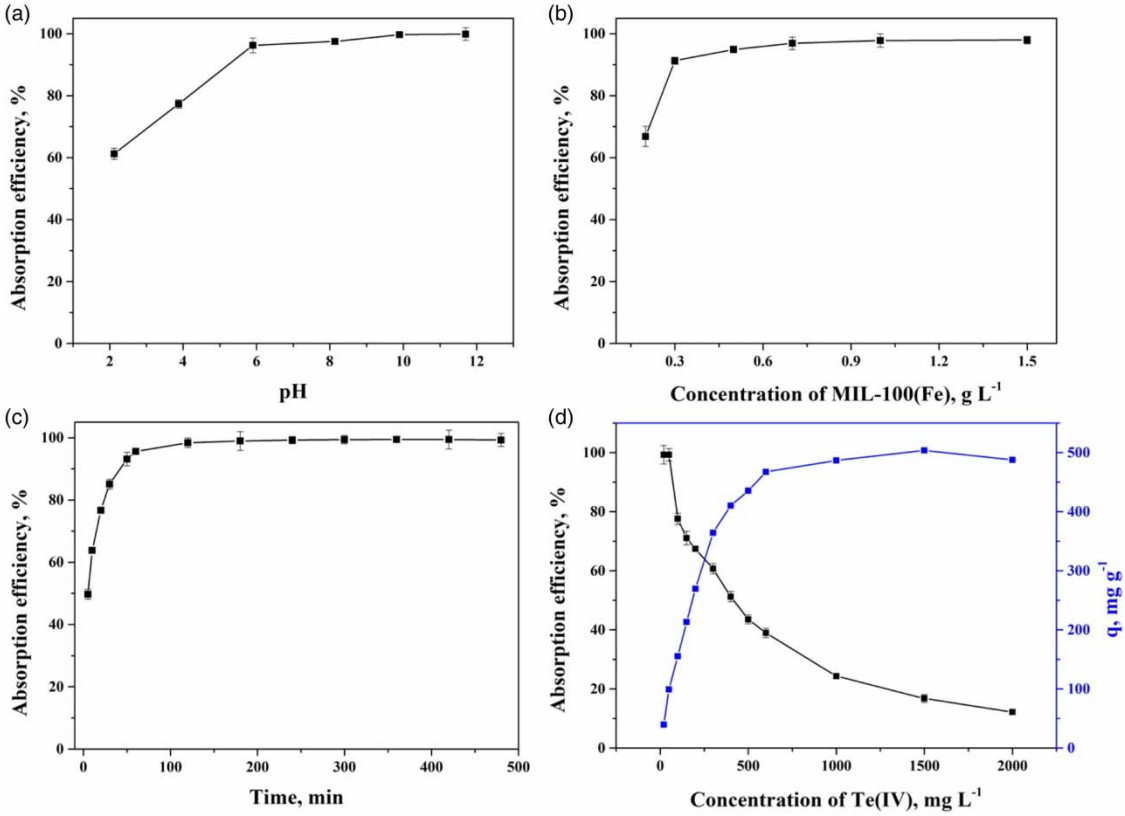

Figure 1 | Effect of solution pH (a) and adsorption dose (b) on the adsorption of Te(IV) by MIL-100(Fe): adsorption time, 2 h; adsorption dose, 0.5 g/L; concentration of Te(IV), 50 mg/L; adsorption temperature: 25 °C; (c) effect of adsorption time on the adsorption of Te(IV) by MIL-100(Fe): adsorption dose, 0.5 g/L; adsorption temperature 25 °C; (d) effect of initial Te(IV) concentration on the adsorption of Te(IV) by MIL-100(Fe): adsorption time, 2 h; adsorption dose, 0.5 g/L; adsorption temperature: 25 °C.

The amount of adsorbent is a significant element in the analyte's quantitative adsorption, which directly determines the adsorption sites' quantity. Choosing the optimal amount of adsorbent also has significant implications for the adsorption process efficiency in terms of cost. Therefore, we investigated the impact of the concentration of MIL-100(Fe) on the removal of Te(IV) within the range of 0.2–1.5 g/L. With the elevation in the concentration of the MOF material, the number of adsorption sites also gradually increases, which is conducive to the removal of Te(IV) by the material. As depicted in Figure 1(b), when the amount of adsorbent reaches 0.5 g/L, the removal rate of Te(IV) can reach over 96%, and then kept almost constant. This phenomenon could be owing to the increase in the amount of adsorption sites and the contact area (Ma *et al.* 2020). During the process of Te(IV) adsorption, the number of adsorption sites escalates rapidly as the dosage of the adsorbent increases. However, a portion of these sites remains unsaturated, resulting in a reduced utilization rate of MIL-100(Fe). Considering the removal efficiency and the principle of using minimal reagents to reduce experimental costs, the amount of MIL-100(Fe) adsorbent chosen for subsequent experiments was 0.5 g/L.

The contact time between the solid-phase material and the target analyte to some extent affects the efficiency of element removal. Therefore, this study examined the impact of adsorption time on the Te(IV) removal process. As shown in Figure 1(c), within 0–60 min, the removal efficiency of Te(IV) by MIL-100(Fe) rapidly increases with the extension of adsorption time, and at 60 min, a removal efficiency exceeding 90% is achieved. It may be due to the rich adsorption sites on the surface of MIL-100(Fe), making for a rapid increase in the adsorption efficiency of MIL-100(Fe). And the adsorption equilibrium was attained with a maximum adsorption efficiency of 98% after 2 h. This was caused by the exhaustion of numerous adsorption sites on the MIL-100(Fe) surface. Besides, as the reaction proceeds, spatial resistances was increased and electron transfer rates were reduced, which in turn diminishes the ability to bind with Te(IV), resulting in a slight increase in adsorption time. Therefore, a reaction time of 2 h was chosen for subsequent experiments. Furthermore, the initial concentration of Te(IV) is a crucial factor involved in assessing the adsorption performance of the adsorbent and its performance in a

real-world setting. Subsequently, we studied the impact of high-concentration Te(IV) initial concentration on the adsorption performance of MIL-100(Fe) under the condition of a removal time of 2 h. Figure 1(d) displays the adsorption capacity of MIL-100(Fe) under different Te(IV) concentrations. As the initial Te(IV) concentration continuously rises, the amount of Te(IV) adsorbed by the nanomaterial gradually increases in the range of 5–500 mg/L Te(IV). As the concentration of Te(IV) rises to 1,000 mg/L, the amount of Te(IV) adsorbed by 0.5 g/L MIL-100(Fe) stabilizes, attaining the adsorption capacity of 503.8 mg/g. This could be as a result of the adsorbed Te(IV) covering the adsorption sites on the materials surface as the adsorption amount increased, thereby preventing further adsorption to the unused active sites. According to the above findings, the prepared MIL-100(Fe) material has superior removal capacity for Te(IV).

Impact of competitive ions

Various types of anions exist in environmental waters, and the removal effect of the adsorbent on Te(IV) will be influenced by the types and ion strength in the water. Therefore, we investigated the impact of competitive ions in the water (Ca^{2+}, Mg^{2+}, K^{+}, Na^{+}, NO_3^-, HCO_3^-, PO_4^{3-}, CO_3^{2-}) on the removal of Te(IV) by MIL-100(Fe), as depicted in Table 1. Considering the complexity of the seawater matrix, the types and concentrations of coexisting ions refer to the standard seawater values. The findings show that under the existence of 20,000 mg/L of Na^{+}, 5,000 mg/L of Mg^{2+}, 1,000 mg/L of Ca^{2+} and K^{+}, 400 mg/L of NO_3^-, CO_3^{2-}, and HCO_3^-, and 100 mg/L of PO_4^{3-}, the removal rate of Te(IV) by this adsorbent, MIL-100(Fe), still exceeds 94%. This indicates that MIL-100(Fe) has strong resistance to interference in the system for removing Te(IV), and is expected to be applied to environmental waters of different matrices.

Removal of Te(IV) in actual water samples

Under the selected experimental conditions, we investigated the performance of this material in removing high-concentration Te(IV) in actual environmental water samples. Therefore, we chose lake water, river water, and high-salinity seawater as sample matrices. The seawater matrix was used after diluting the actual seawater by half. To better demonstrate the effect of MIL-100(Fe) in removing Te(IV), we added an additional 20 mg/L Te(IV) into each type of environmental water sample and then conducted the removal experiment. As shown in Table 2, the findings demonstrate that the removal efficiency of this material for Te(IV) in general river or lake water was as high as 99%. And for seawater matrix, the removal efficiency of Te(IV) was over 94%. It may be attributed to the excessive salinity and ionic intensity in the sample solution. This indicates that the adsorbent successfully applies to the effective removal of Te(IV) in environmental waters (including seawater).

Table 1 | Effect of coexisting ions on removal of Te by MIL-100(Fe)

Coexisting ions	Concentrations (mg/L)	Removal efficiency (%)
Mg^{2+}	5,000	99 ± 1
Na^{+}	20,000	94 ± 3
Ca^{2+}	1,000	99 ± 2
K^{+}	1,000	100 ± 2
NO_3^-	400	100 ± 3
CO_3^{2-}	400	96 ± 2
HCO_3^-	400	97 ± 4
PO_4^{3-}	100	96 ± 2

Table 2 | The removal efficiency of Te(IV) from natural water by MIL-100(Fe)

Sample	Removal efficiency (%)
Lake water	99 ± 1
River water	100 ± 1
Dalian seawater	94 ± 1
Hainan sea water	95 ± 3

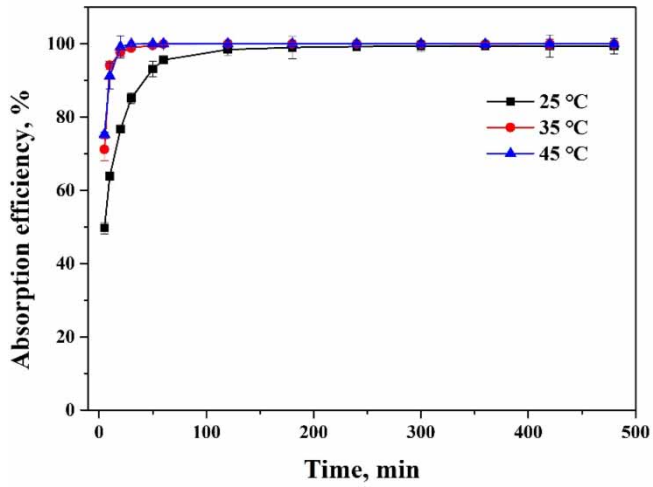

Figure 2 | Effect of adsorption temperature on Te(IV) adsorption: adsorption time, 2 h; adsorption dose, 0.5 g/L; concentration of Te(IV), 50 mg/L.

Adsorption mechanism

This study thoroughly investigated the potential mechanism of MIL-100(Fe) in removing Te(IV). First, under the selected experimental conditions (50 mL of 50 mg/L Te(IV), 0.5 g/L of MIL-100(Fe), pH = 7, adsorption time = 2 h), we explored the impact of reaction temperature (25, 35, 45 °C) on the removal of Te(IV). As depicted in Figure 2, as the reaction temperature rises, the removal efficiency of Te(IV) significantly increases. This indicates that an increase in temperature is beneficial to the adsorption reaction, suggesting that the adsorption process is endothermic.

Adsorption kinetic models describe the rate of solute absorption that controls the contact time of the adsorption reaction and is one of the crucial features in determining the adsorption efficiency. Therefore, we used the pseudo-first-order (PFO) kinetic model and pseudo-second-order (PSO) model to determine the fixation rate of Te(IV) on the adsorbent MIL-100(Fe). Their linear expressions are as follows:

$$\ln(q_e - q_t) = \ln q_e - k_1 t \tag{3}$$

$$\frac{t}{q_t} = \frac{1}{k_2 q_e^2} + \frac{t}{q_e} \tag{4}$$

where k_1 and k_2 are the adsorption rate constants of the PFO kinetics and PSO kinetics, respectively, t is the reaction time, q_e is the adsorption amount at adsorption equilibrium, and q_t is the adsorption amount at this reaction time. According to findings, in this adsorption process, the correlation linear coefficient $R^2 = 0.9999$ of the PSO kinetic model is significantly better in comparison to the correlation linear coefficient $R^2 = 0.8333$ of the PFO (Figure 3). Moreover, the adsorption capacity (q_e = 40 mg g^{-1}) simulated by the PSO kinetic model is nearer to the experimental findings. Therefore, the adsorption process of MIL-100(Fe) for Te(IV) conforms more to the PSO kinetic model, demonstrating that this adsorption process may be mainly chemical adsorption, supplemented by physical adsorption (Azizian 2004; Guo & Wang 2019). Other corresponding fitting results were present in Table S2, Supplementary material.

One of the basic parameters employed to investigate the maximum adsorption capacity is the adsorption isotherm, which effectively defines how the adsorbent and Te(IV) interact. Therefore, the Langmuir (LM) and Freundlich (FL) models were employed in the experiment to simulate the adsorption performance of the adsorbent, with their linear expressions as follows:

$$\frac{C_e}{q_e} = \frac{C_e}{q_m} + \frac{1}{K_L q_m} \tag{5}$$

$$\ln q_e = \ln K_F + \frac{1}{n} \ln C_e \tag{6}$$

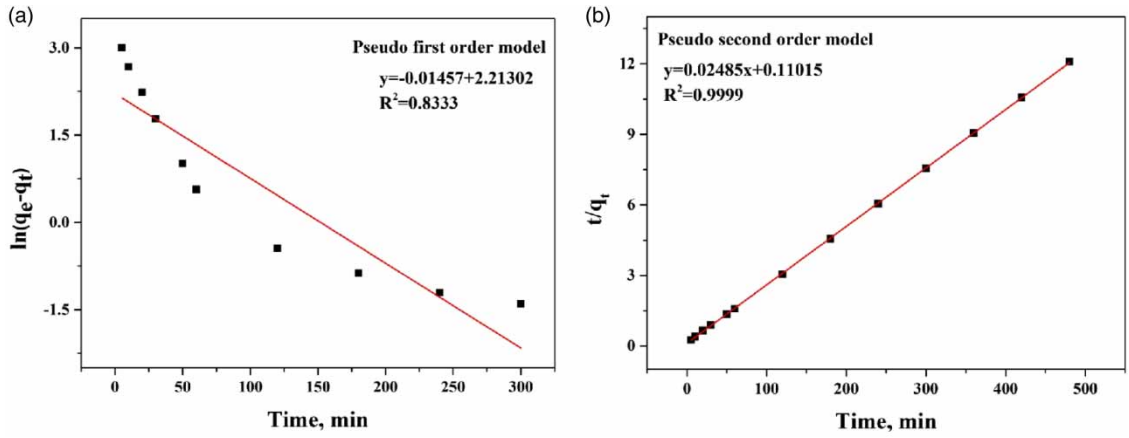

Figure 3 | Kinetics of adsorption of Te(IV) by MIL-100(Fe): pseudo-first-order model (a) and pseudo-second-order model (b).

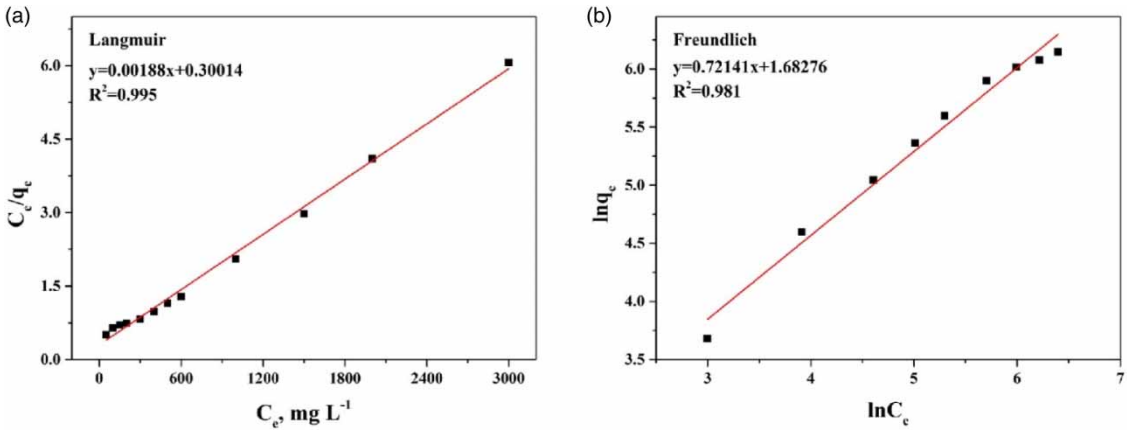

Figure 4 | Langmuir (a) and Freundlich (b) adsorption isotherm plot in a linear form for Te(IV) adsorption onto MIL-100(Fe).

where $1/n$ is a constant representing the adsorption capacity, K_L and K_F are the LM and FL constants, respectively, C_e is the concentration at equilibrium, q_e is the adsorption amount at equilibrium, and q_m is the maximum adsorption amount after equilibrium. The fitted results show that the correlation coefficient $R^2 = 0.995$ of the LM model is close to 1, significantly better than the correlation linear coefficient $R^2 = 0.981$ of the FL model (Figure 4), indicating that the adsorption process should belong to the monolayer chemical adsorption (Al-Ghouti & Da'ana 2020). This is consistent with the findings of the PSO kinetic model, suggesting that the adsorption of Te(IV) by MIL-100(Fe) is mainly due to chemical adsorption. The maximum adsorption capacity of Te(IV), q_m, was calculated to be 531.90 mg g^{-1}. Compared with other materials for the adsorption of Te(IV), this material has better adsorption performance for Te(IV) than other adsorbents (Table 3).

The experiment used SEM-EDS to characterize the surface morphology and elemental content of MIL-100(Fe) after adsorption. As depicted in Figure 5, after MIL-100(Fe) adsorbed Te(IV), it significantly aggregated (Figure 5(a) and 5(e)). Elements such as C, O, and Fe are well distributed on the MIL-100(Fe) surface, and by comparing with the distribution and content of surface elements before adsorption, Te(IV) can be clearly observed to be attached to the MIL-100(Fe) surface after adsorption (Figure 5(h)). This proves that the prepared adsorbent can effectively remove Te(IV) in the solution through a strong adsorption effect.

To clarify the interaction mechanism between Te(IV) and MIL-100(Fe), the experiment used XPS technology to characterize MIL-100(Fe) pre- and post-adsorption of Te(IV). As depicted in Figure 6(a), after MIL-100(Fe) adsorbed Te(IV) (red line), in addition to the three typical characteristic peaks of C 1 s, O 1 s, and Fe 2p, a clear Te 3d characteristic peak appeared. This

Table 3 | Comparison of adsorption of Te(IV) by different adsorption materials

Adsorbent	pH	q_m (mg/g)	Ref.
Porous Zirconia Microspheres	2–10	18.92	Wu *et al.* (2018)
Magnetic FeS@Lignin-derived carbon nanocomposites	6	108.87	Yao *et al.* (2021b)
ZnO–Ag@Cellulose composite	2–6	29.77	Yao *et al.* (2021a)
MIL-100(Fe)	6–12	531.90	This work

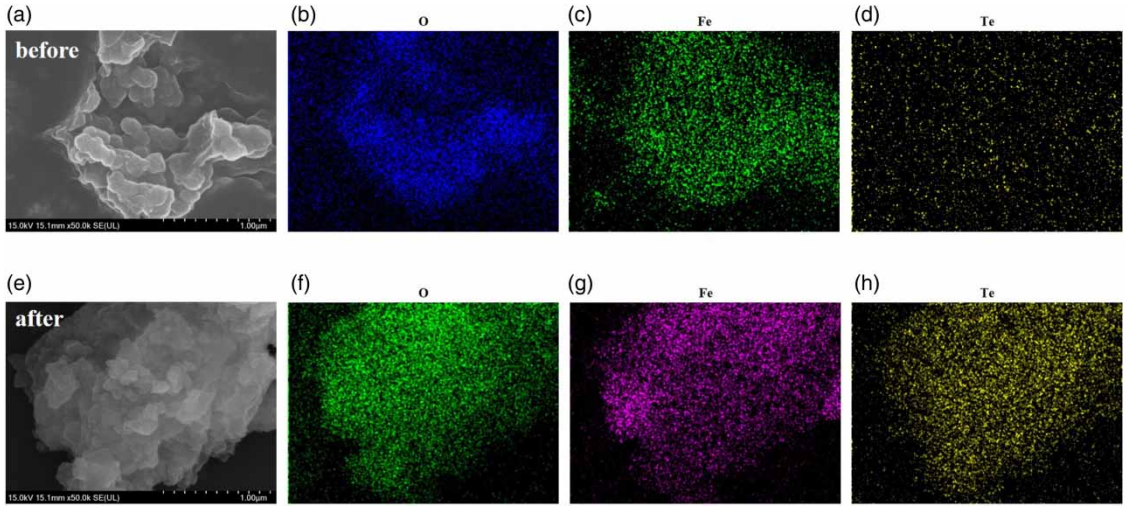

Figures 5 | SEM images and EDS characterization of MIL-100(Fe) before (a–d) and after (e–h) adsorption.

confirms that MIL-100(Fe) effectively adsorbed and removed pollutants through chemical adsorption (Yue *et al.* 2019). By analyzing the characteristic peak generated by Te 3d, it was found that after Te(IV) was adsorbed, its valence state did not change (Figure 6(b)). By peak splitting the high-resolution XPS spectrum of O 1 s, it was found that for MIL-100(Fe) without adsorption reaction, the O1s spectra at 529.8, 531.7, and 533.3 eV were C–O, C–OH, and C = O bonds, respectively (Figure 7(a)) (Li *et al.* 2021a). After the adsorption reaction, the C–O peak moved from 529.8 to 530.4 eV (Figure 7(b)). The peak area of the C–O bond increased significantly, indicating that during the adsorption process, the functional groups with unsaturated bonds on the adsorbent were oxidized, which may promote the formation of Te–O chemical

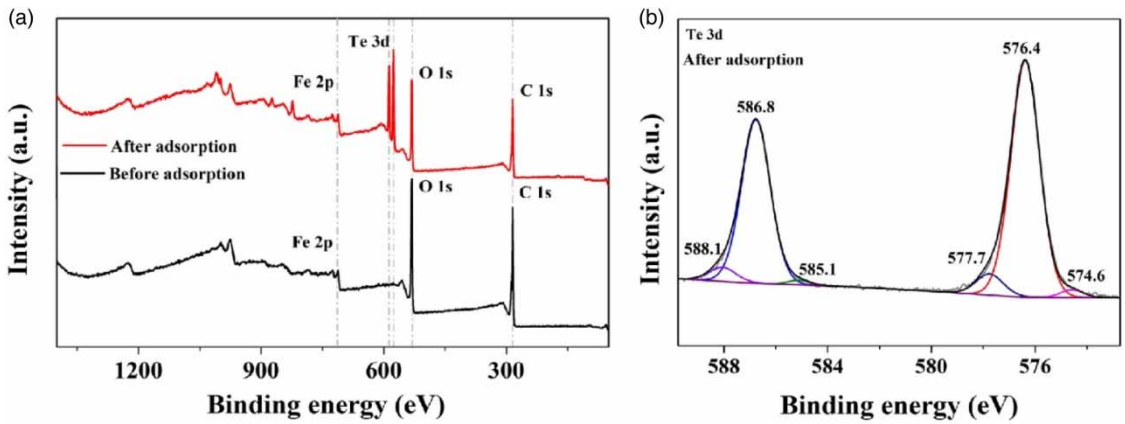

Figure 6 | XPS spectra of MIL-100(Fe): a comparison of the general map before and after adsorption (a); Te 3d XPS spectra after adsorption (b).

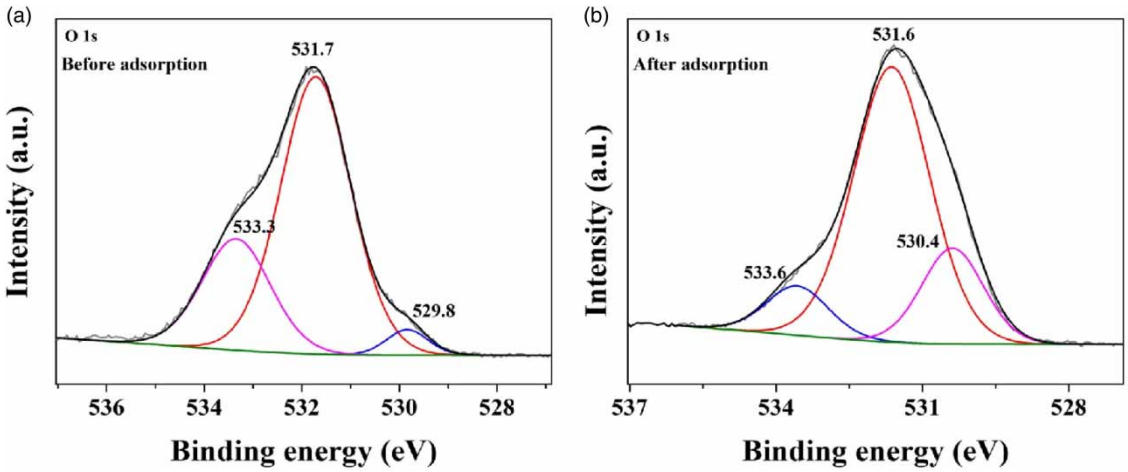

Figure 7 | O 1 s XPS spectra before (a) and after (b) adsorption.

bonds (Yao *et al.* 2021a). This also shows that the adsorption of Te(IV) by this adsorbent is chemical adsorption, consistent with the results of kinetic analysis.

CONCLUSION

This research proposed the first-time use of the MOF material MIL-100(Fe) to remove Te(IV) from environmental aquatic systems. The material achieved adsorption equilibrium within 2 h and showed a broadly applicable pH range (pH = 6–12). It demonstrated high adsorption capacity (531.9 mg/g) and excellent selectivity for Te(IV) removal, with strong resistance to interference. The adsorption process was primarily a monolayer chemical adsorption and an endothermic reaction. When applied to the removal of high concentrations of Te(IV) in actual lake water, river water, and seawater, the material achieved excellent removal results, confirming its applicability. The material holds the potential for the removal of Te(IV) in other complex matrices.

SUPPORTING INFORMATION

Additional information as noted in text, including XRD patterns of the synthesized MIL-100(Fe), N_2 adsorption and desorption isotherms of MIL-100(Fe), pore diameter distribution profiles of MIL-100(Fe), FTIR spectra of MIL-100(Fe) microspheres before and after adsorption, ICP-OES operating conditions and kinetics and isotherm model parameters of adsorption of Te(IV) by MIL-100(Fe).

ACKNOWLEDGEMENTS

Sichuan Province Science and Technology Support Program (No. 2023NSFSC0753) and Natural Science Foundation of Sichuan Province (No. 2022NSFSC1902) are acknowledged for their financial support.

DATA AVAILABILITY STATEMENT

All relevant data are included in the paper or its Supplementary Information.

CONFLICT OF INTEREST

The authors declare there is no conflict.

REFERENCES

Al-Ghouti, M. A. & Da'ana, D. A. 2020 Guidelines for the use and interpretation of adsorption isotherm models: A review. *Journal of Hazardous Materials* **393**, 122383.

Arab, F., Mousavi-Kamazani, M. & Salavati-Niasari, M. 2017 Facile sonochemical synthesis of tellurium and tellurium dioxide nanoparticles: Reducing Te(IV) to te via ultrasonic irradiation in methanol. *Ultrasonics Sonochemistry* **37**, 335–343.

Azizian, S. 2004 Kinetic models of sorption: A theoretical analysis. *Journal of Colloid And Interface Science* **276** (1), 47–52.

Belzile, N. & Chen, Y. W. 2015 Tellurium in the environment: A critical review focused on natural waters, soils, sediments and airborne particles. *Applied Geochemistry* **63**, 83–92.

Borner, F., Keith, M., Smith, D. J., Barry, T. L., Neumann, T. & Klemd, R. 2021 Fingerprinting fluid evolution by trace elements in epithermal pyrite, vatukoula Au-Te deposit, Fiji. *Ore Geology Reviews* **137**, 104314.

Cai, J., Wang, X., Zhou, Y., Jiang, L. & Wang, C. 2016 Selective adsorption of arsenate and the reversible structure transformation of the mesoporous metal-organic framework MIL-100(Fe). *Physical Chemistry Chemical Physics* **18** (16), 10864–10867.

Chen, H., Xu, J., Li, Y., Zhang, T., Qiu, F. & Huang, X. 2021 Trash to treasure: From construction waste to tellurium adsorbent materials. *Journal of Cleaner Production* **312**, 127752.

Dubey, S., Banerjee, S., Upadhyay, S. N. & Sharma, Y. C. 2017 Application of common nano-materials for removal of selected metallic species from water and wastewaters: A critical review. *Journal of Molecular Liquids* **240**, 656–677.

Guo, X. & Wang, J. 2019 A general kinetic model for adsorption: Theoretical analysis and modeling. *Journal of Molecular Liquids* **288**, 111100.

Gupta, V. K., Gupta, B., Rastogi, A., Agarwal, S. & Nayak, A. 2011 A comparative investigation on adsorption performances of mesoporous activated carbon prepared from waste rubber tire and activated carbon for a hazardous azo dye–acid blue 113. *Journal of Hazardous Materials* **186** (1), 891–901.

Hasan, Z. & Jhung, S. H. 2015 Removal of hazardous organics from water using metal-organic frameworks (MOFs): Plausible mechanisms for selective adsorptions. *Journal of Hazardous Materials* **283**, 329–339.

Jun, J. W., Tong, M., Jung, B. K., Hasan, Z., Zhong, C. & Jhung, S. H. 2015 Effect of central metal ions of analogous metal–organic frameworks on adsorption of organoarsenic compounds from water: Plausible mechanism of adsorption and water purification. *Chemistry–A European Journal* **21** (1), 347–354.

Ke, F., Wang, L. & Zhu, J. 2015 Facile fabrication of CdS-metal-organic framework nanocomposites with enhanced visible-light photocatalytic activity for organic transformation. *Nano Research* **8**, 1834–1846.

Kim, S., Lee, J., Son, Y. & Yoon, M. 2020 Study of the dye adsorption kinetics of metal-organic frameworks in aqueous media. *Bulletin of the Korean Chemical Society* **41** (8), 843–850.

Kreno, L. E., Leong, K., Farha, O. K., Allendorf, M., Van Duyne, R. P. & Hupp, J. T. 2012 Metal-organic framework materials as chemical sensors. *Chemical Reviews* **112** (2), 1105–1125.

Li, J., Wu, Y.-n., Li, Z., Zhang, B., Zhu, M., Hu, X., Zhang, Y. & Li, F. 2014 Zeolitic imidazolate framework-8 with high efficiency in trace arsenate adsorption and removal from water. *The Journal of Physical Chemistry C* **118** (47), 27382–27387.

Li, J., Wang, X., Zhao, G., Chen, C., Chai, Z., Alsaedi, A., Hayat, T. & Wang, X. 2018 Metal-organic framework-based materials: Superior adsorbents for the capture of toxic and radioactive metal ions. *Royal Society of Chemistry Chemical Society Reviews* **47** (7), 2322–2356.

Li, L., Wu, H., Chen, J., Xu, L., Sheng, G., Fang, P., Du, K., Shen, C. & Guo, X. 2021a Anchoring nanoscale iron sulfide onto graphene oxide for the highly efficient immobilization of uranium (VI) from aqueous solutions. *Journal of Molecular Liquids* **332**, 115910.

Li, Z., Gou, M., Yue, X., Tian, Q., Yang, D., Qiu, F. & Zhang, T. 2021b Facile fabrication of bifunctional ZIF-l/cellulose composite membrane for efficient removal of tellurium and antibacterial effects. *Journal of Hazardous Materials* **416**, 125888.

Li, Z., Qiu, F., Yue, X., Tian, Q., Yang, D. & Zhang, T. 2021c Eco-friendly self-crosslinking cellulose membrane with high mechanical properties from renewable resources for oil/water emulsion separation. *Journal of Environmental Chemical Engineering* **9** (5), 105857.

Liu, Y., Liu, P., Jiang, Q., Jiang, F., Liu, J., Liu, G., Liu, C., Du, Y. & Xu, J. 2021 Organic/inorganic hybrid for flexible thermoelectric fibers. *Chemical Engineering Journal* **405**, 126510.

Ma, L., Chen, N., Feng, C., Li, M., Gao, Y. & Hu, Y. 2020 Coupling enhancement of chromium (VI) bioreduction in groundwater by phosphorus minerals. *Chemosphere* **240**, 124896.

Narimani-Sabegh, S. & Noroozian, E. 2018 Magnetic solid-phase extraction with copper ferrite nanoparticles for the separation and preconcentration of ultra-trace amounts of tellurium (IV) ion in aqueous samples. *Journal of the Iranian Chemical Society* **16** (1), 73–81.

Qiu, Z., Wang, M., Zhang, T., Yang, D. & Qiu, F. 2020 In-situ fabrication of dynamic and recyclable TiO_2 coated bacterial cellulose membranes as an efficient hybrid absorbent for tellurium extraction. *Cellulose* **27** (8), 4591–4608.

Tahmasebi, E., Masoomi, M. Y., Yamini, Y. & Morsali, A. 2015 Application of mechanosynthesized azine-decorated zinc(II) metal-organic frameworks for highly efficient removal and extraction of some heavy-metal ions from aqueous samples: A comparative study. *Inorganic Chemistry* **54** (2), 425–433.

Wang, X. & Dai, S. 2009 A simple method to ordered mesoporous carbons containing nickel nanoparticles. *Adsorption* **15** (2), 138–144.

Wang, M., He, J., Luo, J., Hu, J. & Hou, X. 2022 Ultrasensitive determination and non-chromatographic speciation of inorganic arsenic in foods and water by photochemical vapor generation-icpms using CdS/MIL-100 (Fe) as adsorbent and photocatalyst. *Food Chemistry* **375**, 131841.

Wu, X., Guo, X. & Zhang, L. 2018 Fabrication of porous zirconia microspheres as an efficient adsorbent for removal and recovery of trace Se(IV) and Te(IV). *Industrial & Engineering Chemistry Research* **58** (1), 342–349.

Xu, Z., Guo, X., Li, D., Tian, Q. & Zhu, L. 2020 Selective recovery of Sb and Te from the sodium sulfide leach solution of te-bearing alkaline skimming slag by drop-wise H_2O_2 addition followed by Na_2S–Na_2SO_3 precipitation. *Hydrometallurgy* **191**, 105219.

Xue, H., Chen, Q., Jiang, F., Yuan, D., Lv, G., Liang, L., Liu, L. & Hong, M. 2016 A regenerative metal-organic framework for reversible uptake of Cd(II): From effective adsorption to in situ detection. *Chemical Science* **7** (9), 5983–5988.

Yao, G., Shao, X., Qiu, Z., Qiu, F. & Zhang, T. 2021a Hierarchical flower-like ZnO-Ag@cellulose composite with antifouling and antibacterial properties for efficient recovery of tellurium (IV) from wastewater. *Cellulose* **28** (9), 5719–5734.

Yao, G., Wang, K., Wang, M., Shao, X., Qiu, F. & Zhang, T. 2021b Magnetic FeS@lignin-derived carbon nanocomposites as an efficient adsorbent for multistage collaborative selective recovery of tellurium (IV) from wastewater. *Journal of Environmental Chemical Engineering* **9** (5), 106135.

Yu, H., Chu, Y., Zhang, T., Yu, L., Yang, D., Qiu, F. & Yuan, D. 2018 Recovery of tellurium from aqueous solutions by adsorption with magnetic nanoscale zero-valent iron (NZVFe). *Hydrometallurgy* **177**, 1–8.

Yu, F., Wang, L., Xing, Q., Wang, D., Jiang, X., Li, G., Zheng, A., Ai, F. & Zou, J. P. 2020 Functional groups to modify g-c_3n_4 for improved photocatalytic activity of hydrogen evolution from water splitting. *Chinese Chemical Letters* **31** (6), 1648–1653.

Yue, X., Chen, H., Zhang, T., Qiu, Z., Qiu, F. & Yang, D. 2019 Controllable fabrication of tendril-inspired hierarchical hybrid membrane for efficient recovering tellurium from photovoltaic waste. *Journal of Cleaner Production* **230**, 966–973.

Zhang, L., Zhang, M., Guo, X., Liu, X., Kang, P. & Chen, X. 2010 Sorption characteristics and separation of tellurium ions from aqueous solutions using nano-TiO_2. *Talanta* **83** (2), 344–350.

Zhao, S., Huang, W., Xie, J., Liu, W., Qu, Z. & Yan, N. 2021 Mercury removal from flue gas using UiO-66-type metal-organic frameworks grafted with organic functionalities. *Fuel* **289**, 119807.

First received 17 September 2023; accepted in revised form 25 December 2023. Available online 9 January 2024